**ARTICLE**

# Smart Colorimetric Corn Starch Films Combined with Anthocyanin-Loaded Glutenin-Carboxymethyl Chitosan Nanocomplexes for Freshness Monitoring of Chilled Pork

**Juan Yan[1], Wenchao Li[1], Xianfang Zhang[1] and Shisheng Liu[2,*]**

[1]College of Food Science and Engineering, Hainan University, Haikou, 570100, China

[2]Engineering Research Center for Utilization of Tropical Polysaccharide Resources, Ministry of Education, Haikou, 570100, China

*Corresponding Author: Shisheng Liu. Email: stoneliu77@hainanu.edu.cn

## ABSTRACT

In this study, intelligent, pH-responsive colorimetric films were prepared by encapsulating anthocyanins in nanocomplexes prepared from glutenin and carboxymethyl chitosan. These nanocomplexes were added to a corn starch matrix and used in the freshness monitoring of chilled pork. The effects of anthocyanin-loaded nanocomplexes on the physical, structural, and functional characteristics of the films were investigated. The addition of anthocyanin-loaded nanocomplexes increased the tensile strength, elongation at break, hydrophobicity, and light transmittance of the films while decreasing their water vapor permeability. This is because new hydrogen bonds are formed between the film components, resulting in a more homogeneous and dense structure. The colorimetric film has a significant color response to pH changes. These films were used in experiments on the freshness of chilled pork, in which the pH changes with changing freshness states. The results show that the colorimetric film can monitor changes in the freshness of chilled pork in real time, where orange, pink, and green represent the fresh, secondary fresh, and putrefied states of pork, respectively. Therefore, the intelligent colorimetric film developed in this study has good application potential in the food industry.

## KEYWORDS

Carboxymethyl chitosan; glutenin; nanocomplexes; anthocyanins; pH indicator film; chilled pork

## 1 Introduction

Traditional food packaging acts as a barrier between food and the environment, shielding it from the elements and extending the life of the food [1]. However, the primary raw materials used to make food product films are conventional synthetic polymers derived from petroleum, which have serious environmental implications [2,3]. Presently, with increasing awareness of environmental issues and food safety, the development of biodegradable smart packaging films has garnered great interest from the greater public [4]. As a result, a variety of natural biopolymers, such as proteins, lipids, and polysaccharides, have been employed to create food packaging films [5]. Materials that can monitor how packaged food is being stored and provide information as to its freshness are referred to as smart packaging. In the food business, there has been an increase in interest in the topic of smart packaging [6,7].

Anthocyanins (ACNs) are naturally derived colorants and antioxidants, with potent antioxidant and anti-microbial properties [8]. ACN-rich films are therefore beneficial in conserving the quality of food goods and extending their storability [9]. As ACNs are pH-sensitive and can alter their chemical characteristics and color according to the pH, they can be used to check the quality of some food products in real time [10,11]. However, pH effects may cause ACNs to leach and degrade, owing to their low chemical stability, which limits their application in the food industry [12]. To make it easier to apply ACN-rich smart packaging films, it is crucial to increase ACN stability.

Encapsulation not only protects unstable ACNs, but also allows for their sustained and controlled release [13]. Nano-composite systems, composed of proteins and polysaccharides, are especially useful encapsulation techniques for improving the stability of ACNs. In most cases, proteins and polysaccharides with opposing charges interact electrostatically to produce protein-polysaccharide nanocomplexes. Casein and carboxymethylcellulose nanocomplexes encapsulated with ACNs prepared by electrostatic interactions effectively attenuate the degradation of ACNs under harsh environments [14]. Zhang et al. created nanocarriers using ovalbumin and propylene glycol alginate to protect and gradually release ACNs [15].

Rubber seeds, as a by-product of rubber trees, are discarded in the woods except for a small amount for propagation and fodder, causing a great waste of plant protein resources; recycling rubber seeds would greatly increase the economic value of rubber trees [16,17]. Glutenin, extracted from rubber seeds, is widely available, inexpensive, and readily soluble in dilute acids and bases. Its high content of hydrophobic amino acids helps to stabilize the internal structure of glutenin. pH influences glutenin's surface potential, making it positively charged under acidic conditions. Carboxymethyl chitosan (CMC), a biodegradable natural polysaccharide, is a biopolymer widely used in biomedical, pharmaceutical, and food applications owing to its non-toxicity, biocompatibility, and antimicrobial properties [18,19]. CMC has also been used to prepare nanocomplexes for the protection of bioactive substances. For example, Liu et al. used CMC and chitosan hydrochloride to prepare nanocomplexes to protect stilbene-glycosides [20]. To encapsulate ACNs and increase their stability, glutenin-carboxymethyl chitosan (G-CMC) nanocomplexes can be created by electrostatic interactions between positively charged glutenin and negatively charged CMC. Starch is a widely used food packaging film material because of its abundance, inexpensiveness, good processability, and excellent film-forming properties. Therefore, it was used as a matrix to construct biodegradable smart films [21,22].

In this study, waste rubber seeds were recycled and for the first time, protein-polysaccharide nanocomplexes were developed from glutenin and CMC and used to encapsulate ACNs. In order to prepare biodegradable smart films, the obtained ACN-loaded protein–polysaccharide nanocomplexes were combined with a starch matrix. The mechanical characteristics, water resistance, light transmittance, and antioxidant capacity of the colorimetric films as well as their structure were characterized. Finally, their practicality was validated by monitoring the freshness of chilled pork.

## 2 Materials and Methods

### 2.1 Materials

Blueberry ACNs (purity: 5%–25%) were purchased from Shanghai McLean Biochemical Technology Co., Ltd. (Shanghai, China). Corn starch (purity ≥ 98%) and CMC (degree of carboxylation ≥ 80%) were acquired from Shanghai Yuanye Bio-Technology Co., Ltd. (Shanghai, China). Analytical grade glycerol, citric acid monohydrate, and ethanol were obtained from Xilong Chemical Co., Ltd. (Guangdong, China).

### 2.2 Extraction of Glutenin in Rubber Seeds

Sun-dried rubber seeds were hulled, crushed, sieved (0.425 mm), and defatted with acetone at a ratio of 1:3 (m/V). The defatted powder was mixed in a 1:10 (m/V) ratio with distilled water, 0.1 mol/L NaCl

solution, 70% ethanol, and distilled water. Using a magnetic stirrer, the solution was agitated for 1 h before centrifuging it for 15 min at 6,000 r/min. After separating the precipitate, the extraction process was carried out twice. Following this, the precipitate was stirred with a 0.05 mol/L NaOH solution at a ratio of 1:16 (m/V) at 55°C for 2 h using a magnetic stirrer and then centrifuged at 6,000 r/min for 15 min to extract the supernatant. The supernatant was adjusted to pH 4.8 with 0.1 mol/L hydrochloric acid solution, then left at 25°C for 4 h, and finally, centrifuged at 8,000 r/min for 20 min to extract the precipitate (glutenin).

### 2.3 Color and Ultraviolet Spectroscopy of ACN Solution

The ultraviolet spectroscopy of ACN solutions under pH of 2–12 was measured using an enzyme marker (Synergy LX; BIOTEK INSTRUMENTS, USA). The colors of the ACN solutions at different pH values were recorded using a camera.

### 2.4 Preparation of Nanocomplexes

The glutenin solution was created by dispersing 2.4 g of glutenin in 50 mL of 0.2 M citric acid solution. This solution was magnetically stirred for 1 h at 55°C, followed by centrifugation to obtain the supernatant. G-CMC nanocomplexes were created by combining CMC (2%) solution with the glutenin solution, at a ratio of 1:1, and stirring at room temperature for 1 h. Blueberry ACN was mixed with the G-CMC nanocomplex solution at a final concentration of 3 mg/mL, magnetically stirred for 90 min, and centrifuged. The supernatant was taken to obtain the G-CMC-ACN nanocomplexes [23].

### 2.5 Characterization of Nanocomplexes

Dynamic light scattering (DLS) was performed using a Zetasizer nano ZS90 (Malvern Instruments, UK) to estimate the average particle size (Dz), zeta potential, and polydispersity index (PDI) of the prepared nanocomplexes.

ACN content was measured by the pH-differential method using an ultraviolet–visible (UV–vis) spectrophotometer (UV-5500PC, METASH, China), according to He et al. [24]. The lyophilized samples (300 mg) were mixed with 3 mL of deionized water and dispersed using a Vortex Mixer. Anhydrous ethanol (27 mL) was added to the mixture to facilitate extraction. After 5 min, the mixture was filtered through a 0.45 μm Millipore membrane to determine the total ACN content (TAC). The free ACN content (FAC) was determined by adding 30 mL of anhydrous ethanol to the 300 mg lyophilized sample, then vortexed for 30 s and filtered through a 0.45 μm Millipore membrane [15]. The following equation was used to compute the encapsulation efficiency (EE):

$$EE(\%) = \frac{TAC - FAC}{TAC} \times 100\% \tag{1}$$

### 2.6 Formation of the Films

A corn starch solution (8% w/v) was gelatinized at 95°C for 15 min and rapidly stirred to reduce the temperature to 25°C. The film forming solution was prepared using the following method:

G-CMC-ACN film: ACN-loaded G-CMC nanocomplexes were added to the gelatinized corn starch solution at a 1:1 ratio, followed by glycerol (30% by mass of corn starch). The solution was stirred continuously for 1 h at approximately 25°C to obtain a film-forming solution containing ACN-loaded G-CMC nanocomplexes.

G-CMC film: The above mentioned method was used but no ACNs were loaded onto the G-CMC nanocomplexes.

A film: The above mentioned method was used, but the ACN-loaded G-CMC nanocomplexes were replaced with an equal amount of ACN aqueous solution (in unpackaged form, 3 mg/mL) to prepare the film-forming solution.

C film: The above mentioned method was used, but the ACN-loaded G-CMC nanocomplexes were replaced with distilled water in the film-forming solution.

The film-forming solution (25 mL) was transferred to a square plastic Petri dish (13 cm × 10 cm × 2.5 cm) and then placed in an oven at 35°C for 12 h. Dry films were stored at 25°C and 50% relative humidity [25].

### 2.7 Characterization of the Films

#### 2.7.1 Scanning Electron Microscope (SEM)

The film samples fractured in liquid nitrogen were fixed on a conductive adhesive, coated with gold, and observed using a field emission SEM (Verios G4 UC, Thermo Fisher Scientific, USA).

#### 2.7.2 X-Ray Diffraction (XRD)

The crystallinity of the samples was measured using an XRD (Smart Lab, RIGAKU, Japan). XRD patterns were collected in the range of 2θ (5°–80°) at a scanning speed of 1°/min.

#### 2.7.3 Fourier Transform Infrared (FTIR) Spectroscopy Analysis

FTIR spectra of the film samples were obtained using an FTIR spectrometer (Tensor 27, Bruker, Germany) in the range of 4,000–400 cm$^{-1}$.

#### 2.7.4 Mechanical Property

The thicknesses of the four types of films were measured using a hand-held electronic micrometer (awt-chy01, EVERTE, China). Five points on the sample were randomly selected for the measurement. The precision of the thickness measurement was 0.001 mm.

The tensile strength (TS) and elongation at break (EAB) of the films were measured using a tensile testing machine (3343; Instron, USA). The film was cut into 2 cm × 10 cm pieces and fixed in place using a fixture. The distances between the fixtures were set to 40 mm and the test speed was 1 mm/s [26]. TS and EAB were calculated as follows:

$$TS \ (MPa) = \frac{F}{a \times b} \tag{2}$$

$$EAB \ (\%) = \frac{L - L_0}{L_0} \times 100\% \tag{3}$$

where $F$ denotes the maximum load (N), $a$ the thickness of the film (mm), $b$ the width of the film (mm), $L$ the length of the film rupture (mm), and $L_0$ the initial length of the film (mm).

#### 2.7.5 Water Resistance

The samples were cut into 2 cm × 2 cm pieces, weighed ($M_1$), and dried at 105°C until the pieces reached a constant weight ($M_2$). The dried films were placed in a weighing dish containing 30 mL of deionized water for 24 h. The undissolved films were dried at 105°C until they reached a constant weight ($M_3$). The moisture content (MC) and water solubility (WS) were calculated using the following equations:

$$MC(\%) = \frac{M_1 - M_2}{M_1} \times 100\% \tag{4}$$

$$WS(\%) = \frac{M_2 - M_3}{M_1} \times 100\% \tag{5}$$

The water vapor permeability (WVP) of the films was measured according to Xiao et al. [27]. In a beaker containing 15 mL of deionized water; the film was secured with a rubber band. At 25°C, the beaker was placed in a desiccator filled with anhydrous silica gel. Every 2 h, the weight of the beaker was recorded. The WVP was calculated using the equation below:

$$WVP(\%) = \frac{\Delta M \times d}{A \times \Delta t \times \Delta P} \times 100\% \tag{6}$$

where $\Delta M$ denotes the change in weight of the beaker (g), $d$ the thickness of the film (m), $A$ the permeation area of the film (m$^2$), $\Delta t$ the testing time (s), and $\Delta P$ the saturated vapor pressure at 25°C.

The film water contact angle (WCA) was measured using a video optical contact angle measuring instrument (OCA20, Dataphysics, Germany). Deionized water (1 μL) was dripped onto the film sample. An image of the droplet was captured by the camera and the angle was measured using the software.

### 2.7.6 Color and Light Transmission

The color parameters of the films were determined using a colorimeter (CR-400; Konica Minolta, Japan) [28]. The total chromatic aberration (ΔE) was calculated as follows:

$$\Delta E = \left[ \left(L^* - L_0^*\right)^2 + \left(a^* - a_0^*\right)^2 + \left(b^* - b_0^*\right)^2 \right]^{0.5} \tag{7}$$

where $L^*$, $a^*$, and $b^*$ are films' color parameters, and $L_0^*$, $a_0^*$, and $b_0^*$ are the color parameters of a standard white board.

The transmittance spectrum of the film was determined using a UV–vis spectrophotometer (UV-5500PC; METASH, China). An empty cuvette was used to set the spectrophotometer to zero before starting the experiment. The film was cut into a 0.8 cm × 4 cm sized piece and pressed to one side of the colorimetric plate. The film's transmittance was measured in the 200–800 nm wavelength range.

### 2.7.7 Antioxidant Properties

The DPPH and ABTS radical scavenging techniques were combined to assess the films' antioxidant properties. The absorbance was measured at 517 nm by mixing 1 mL of the film solution with 4 mL of DPPH methanol solution, and incubating in the dark for 30 min at 25°C. Additionally, 100 μL of film solution was mixed with 3.8 mL of ABTS methanol solution and incubated in the dark for 6 min at 25°C. The absorbance was measured at 734 nm. Antioxidant activity was expressed by calculating the vitamin C equivalent antioxidant capacity (VCEAC) [29].

### 2.7.8 Thermal Properties

The thermal properties of the film samples were evaluated from 30°C to 500°C using a thermogravimetric analyzer (Q600, TA, USA) with a heating rate of 10 °C/min.

### 2.7.9 Color Reaction in Different pH

Different smart films were immersed in the pH buffer solution (pH 2–12) for 1 min each time and the change in film color was measured with a colorimeter (CR-400; Konica Minolta, Japan) [30]. The ΔE was calculated using Eq. (7).

## 2.8 Application

G-CMC-ACN films (6 cm × 2 cm) were fixed over petri dishes containing 10 g of fresh pork, and the containers were sealed using cling film. The petri dishes were refrigerated at 4°C for 10 days. The color of the films was recorded every 2 days. The weight loss rate of the pork was determined by weighing the samples, and the pH and total volatile basic nitrogen (TVB-N) values were determined according to the Chinese standard GB 5009.237-2016 and the automatic Kjeldahl method, respectively [31].

### 2.9 Statistical Analysis

All tests repeated a minimum of three times and the results of the experiments were expressed as the mean ± standard deviation. One-way analysis of variance (ANOVA; $p < 0.05$) was performed on the data using the SPSS23 software to describe the statistical differences between the measurements. All figures were drawn using origin2022b.

## 3 Results and Discussion

### 3.1 Color and Ultraviolet Spectroscopy of ACN Solution

The color changes of ACNs in the pH range of 2.0–12.0 are shown in Fig. 1A. The color of the ACN solution gradually changed from red (pH 2.0) to pink (pH 3.0–4.0) and then faded to colorless as the pH increased (pH 5.0–6.0). As the pH increased, the ACN solution turned purple-brown (pH 7.0–10.0), then yellow-green (pH 11.0–12.0) [23]. The changes in the ultraviolet spectroscopy of the ACN solutions with different pH values are shown in Fig. 1B. The shift of the ACN solution's maximum absorption peak from 515 nm (pH 2.0–6.0) to 580 nm (pH 7.0–12.0) was observed. The color variation and corresponding peak shifts of the ACN solutions are due to the ACNs structural transformation under different pH conditions. ACNs exist as red flavonoid cations in strongly acidic environments; these cations transform into colorless methanol pseudobases in weak acids, and finally change into blue anionic quinone bases and yellow chalcones in alkaline environments [32,33], indicating that blueberry ACN can be used as an indicator.
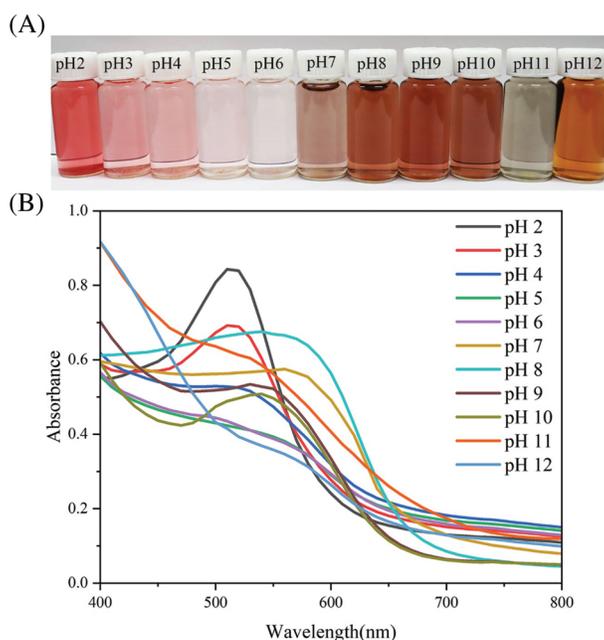


**Figure 1:** Color changes (A) and ultraviolet spectroscopy (B) of ACN solutions at different pH values

### 3.2 Characterization of Nanocomplexes

The Dz, zeta potential, PDI, and EE of the nanocomplexes are shown in Table 1. The Dz of G-CMC-ACN nanocomplexes was significantly larger than that of G-CMC nanocomplexes because ACNs could bind to the G-CMC nanocomplexes through hydrogen bonding or van der Waals forces [34]. The zeta potential is an important parameter for evaluating the stability of nanocomplexes. The addition of ACNs significantly increased the zeta potential of the G-CMC nanocomplexes owing to the flavonoid cations in ACNs.

Consequently, ACN-loaded G-CMC nanocomplexes outperformed G-CMC nanocomplexes in terms of stability. The PDI of the ACN-loaded nanocomplexes was lower than that of the G-CMC nanocomplexes, indicating that the size distribution of ACN-loaded nanocomplexes was more uniform. The EE of ACNs in nanocomplexes was 87.15%, indicating that ACNs can be stably loaded into nanocomplex systems [35].

**Table 1:** Dz, zeta potential, PDI, and EE of nanocomplexes

| Samples | $D_z$ (nm) | Zeta potential (mV) | PDI | EE (%) |
|---|---|---|---|---|
| G-CMC nanocomplexes | $184.87 \pm 3.96$b | $31.63 \pm 0.90$b | $0.52 \pm 0.017$a | — |
| G-CMC-ACN nanocomplexes | $241.9 \pm 6.65$a | $35.37 \pm 1.11$a | $0.301 \pm 0.014$b | $87.15 \pm 1.37$ |

Note: Different letters in the same column indicate significant differences ($p < 0.05$).

### 3.3 Characterization of the Films

#### 3.3.1 SEM Analysis

The microstructures of the four films are shown in Fig. 2A. The cross section of the C film was insufficiently compact, and the surface was rough with big insoluble particles. Compared with the C film, the surface of the film with free ACNs was smaller, and there were fewer large insoluble particles. After the addition of nanocomplexes, the surface of the film became smoother and the cross section became more compact, indicating good biocompatibility between the nanocomplexes and the film matrix [36]. The addition of ACN-loaded nanocomplexes further improved the surface structure of the film, and the cross-section of the film was more uniform and regular. Similar results were found in smart colorimetric films prepared by Liu et al. with ACN-loaded ovalbumin-carboxymethyl cellulose nanocomplexes in a corn starch/polyvinyl alcohol matrix [23]. These findings show that ACN-loaded nanocomplexes greatly enhanced the structure of the film and that ACNs were uniformly distributed in the film.

#### 3.3.2 XRD Analysis

The crystal structures of the four films were analyzed using XRD (Fig. 2B). During gelatinization, the typical A-type crystal structure of corn starch was destroyed, showing only two characteristic peaks ($2\theta = 17.1°$ and $19.9°$). This was due to the recrystallization of starch during film formation and storage. The addition of ACNs or nanocomplexes decreased the signal of the bimodal peaks. When the ACN-loaded nanocomplexes were added, the film showed no new diffraction peak, and formed a diffuse steamed bread peak at $2\theta = 19.9°$, indicating good biocompatibility between the starch and the ACN-loaded nanocomplexes [37]. This was caused by the starch and ACN-loaded nanocomplexes forming intermolecular hydrogen bonds, which prevented the recrystallization of the starch [38].

#### 3.3.3 FTIR Analysis

The infrared spectra of the four films are shown in Fig. 2C. The characteristic peaks of the C film were the O-H stretching vibration at 3421 cm$^{-1}$, C-H stretching vibration at 2931 cm$^{-1}$, O-H bending vibration at 1645 cm$^{-1}$, and glucose pyranose ring vibrations at 1035 and 1087 cm$^{-1}$ [39]. All of the film samples showed the characteristic peaks associated with gelatinized corn starch, indicating that the addition of free ACNs or nanocomplexes had no impact on corn starch's structure and had good biocompatibility [23]. The creation of new hydrogen bonds caused the absorption peak of -OH in the A film to move from 3421 to 3398 cm$^{-1}$ [40]; G-CMC and G-CMC-ACN films' new characteristic peaks at 1724 and 1726 cm$^{-1}$ were caused by nanocomplexes' vibrations of the amide I band (C=O) [41]; simultaneously, peaks at 3421 and 1645 cm$^{-1}$ shifted to 3382 and 1633 cm$^{-1}$, respectively. The peak vibration intensified significantly, indicating the constitution of hydrogen bonds and electrostatic interactions between the ACN-loaded nanocomplexes and film matrix.
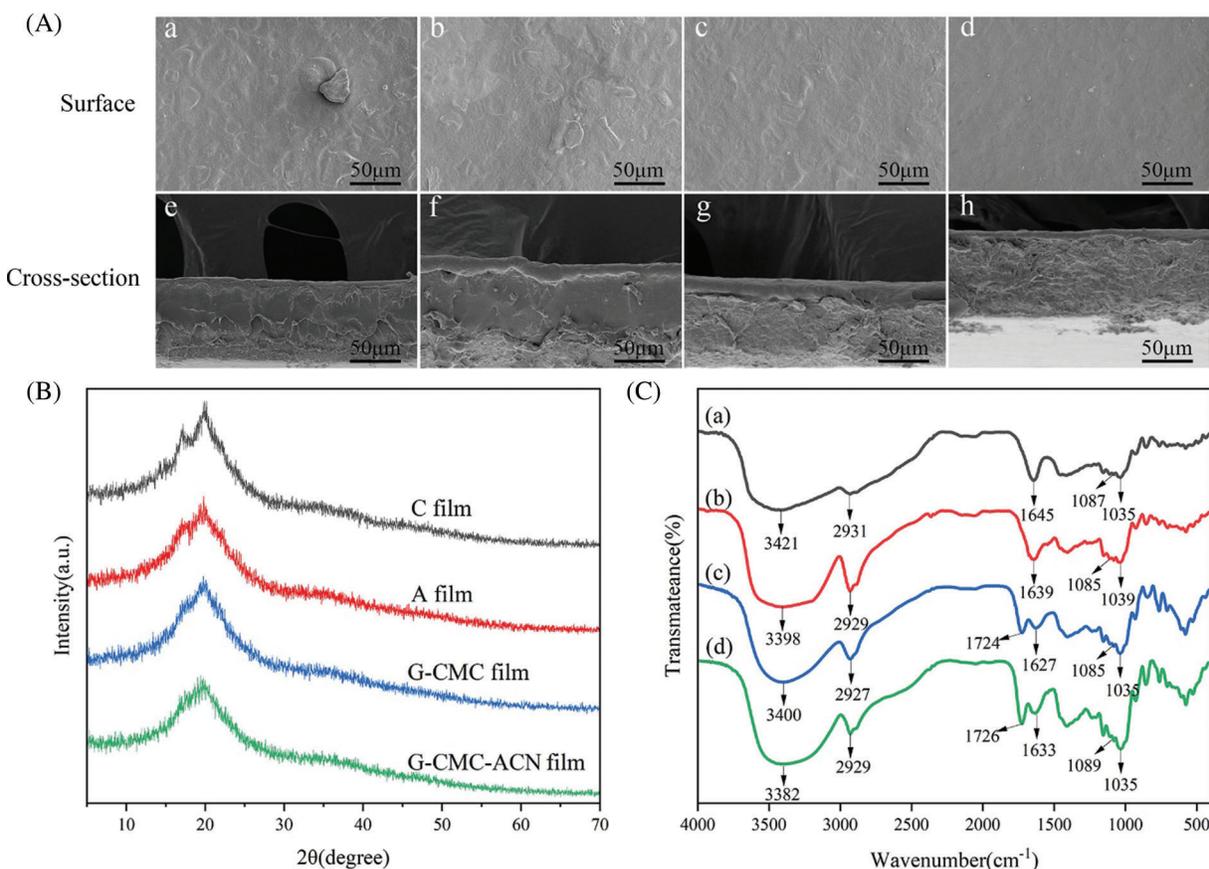
**Figure 2:** Scanning electron microscope (SEM) images of the C (a, e), A (b, f), G-CMC (c, g), and G-CMC-ACN (d, h) films (A). Fourier transform infrared (FTIR) spectrum (B) of the films. X-ray diffraction (XRD) patterns (C) of C (a), A (b), G-CMC (c), and G-CMC-ACN (d) films

### 3.3.4 Mechanical Properties

Table 2 shows the thickness, TS, and EAB of the four films. The four films' thicknesses did not differ significantly ($p > 0.05$), indicating that the addition of ACN or nanocomplexes had no significant effect on film thickness. It is common practice to assess the mechanical characteristics of films using TS and EAB. The addition of free ACN increased the TS ($0.87 \rightarrow 1.83$ MPa) and decreased the EAB ($46.77\% \rightarrow 35.23\%$), as the high rigidity of blueberry ACN decreased the flexibility of the film [42]; however, the addition of ACN-loaded G-CMC nanocomplexes and G-CMC nanocomplexes not only increased the TS from 0.87 to 2.67 MPa and 0.87 to 2.10 MPa, respectively, but also significantly increased the EAB from 46.77% to 93.76% and 46.77% to 182.61%, respectively. Strong interfacial contacts between the G-CMC nanocomplex and the film matrix, which assisted in the formation of the film's dense structure and enhanced its mechanical properties, were responsible for this. The higher TS of G-CMC-ACN films was a consequence of the higher biocompatibility of anthocyanin-loaded nanocomplexes with the film matrix. The lower EAB of G-CMC-ACN films compared to that of G-CMC films was related to the lower chain mobility, as the addition of anthocyanins restricts the movement of polymer chains [43].

**Table 2:** Thickness, MC, WS, TS, EAB, and WVP of films

| Films | Thickness (mm) | Moisture content (%) | Water solubility (%) | TS (MPa) | EAB (%) | WVP ($10^{-11}$g m$^{-1}$s$^{-1}$pa$^{-1}$) |
|---|---|---|---|---|---|---|
| C film | 0.078 ± 0.012a | 25.80 ± 1.13a | 16.96 ± 0.76b | 0.87 ± 0.18d | 46.77 ± 4.30c | 15.85 ± 0.75a |
| A film | 0.083 ± 0.002a | 23.87 ± 1.31ab | 16.87 ± 0.85b | 1.33 ± 0.13c | 35.23 ± 2.24d | 14.19 ± 0.82ab |
| G-CMC film | 0.084 ± 0.005a | 22.82 ± 1.08b | 24.18 ± 0.82a | 2.10 ± 0.14b | 182.61 ± 4.40a | 13.04 ± 1.07b |
| G-CMC-ACN film | 0.080 ± 0.003a | 22.40 ± 0.98b | 25.29 ± 0.75a | 2.67 ± 0.17a | 93.76 ± 5.95b | 10.79 ± 0.41c |

Note: Different letters in the same column indicate significant differences ($p < 0.05$).

### 3.3.5 Water Resistance

The MC, WS, and WVP values of the four films are summarized in Table 2. Owing to the interaction between the hydrophilic hydroxyl groups and water molecules in the pure starch film, the C film had the highest water content (25.80%). The moisture content of the A film did not significantly decrease ($p > 0.05$) after the addition of free ACN. This occurred as some of the water molecules in the film were replaced by ACN molecules [44]. When nanocomplexes were added, the strong interactions between the nanocomplexes and starch reduced the effective number of hydrophilic hydroxy groups, and the water content of the films decreased significantly [42]. The addition of free ACNs did not significantly affect the WS of the films, whereas G-CMC and G-CMC-ACN nanocomplexes increased the WS of the films from 16.96% to 24.18% and from 16.96% to 25.29%, respectively. This is due to the hydrophilic nature of CMC and the weakened cross-linking between polymer molecules when the films swell with water, thus increasing solubility. Free ACNs interact with the hydrophilic groups in the film matrix to generate hydrogen bonds, which lower films' WVP [23]. Owing to the strong interaction between the nanocomplexes and the film matrix, the addition of ACN-loaded G-CMC and G-CMC nanocomplexes effectively diminished the WVP of the films. This made water molecules more resistant to diffusing through the films, and the uniform and compact microstructure restricted the transfer of water in the film matrix [45].

The hydrophilicity/hydrophobicity of the films was evaluated by measuring the water contact angles of the film surfaces; these were hydrophilic when θ < 90° and hydrophobic when θ > 90°. The contact angle of the pure corn starch film was the smallest (WCA = 43.7°; Fig. 3A); the starch film had high hydrophilicity and poor water resistance, because of the multi-hydroxyl structure of starch [46]. As ACNs can form hydrogen bonds with hydrophilic groups in the film matrix, the A film's hydrophilicity was reduced (WCA = 86.2°) [23]. The addition, ACN-loaded G-CMC and G-CMC nanocomplexes improved the hydrophobicity of the films noticeably (WCA = 97.9° and 105.4°, respectively) [12]. This is because the increased interaction between the nanocomplexes and the film matrix hinders the rearrangement of starch chains and makes the surface hydrophobic. The poor water resistance limits the practical applications of the pure starch film. Adding ACNs-loaded G-CMC nanocomplexes is an effective method to improve the water resistance of the film, thereby increasing their suitability for practical applications.
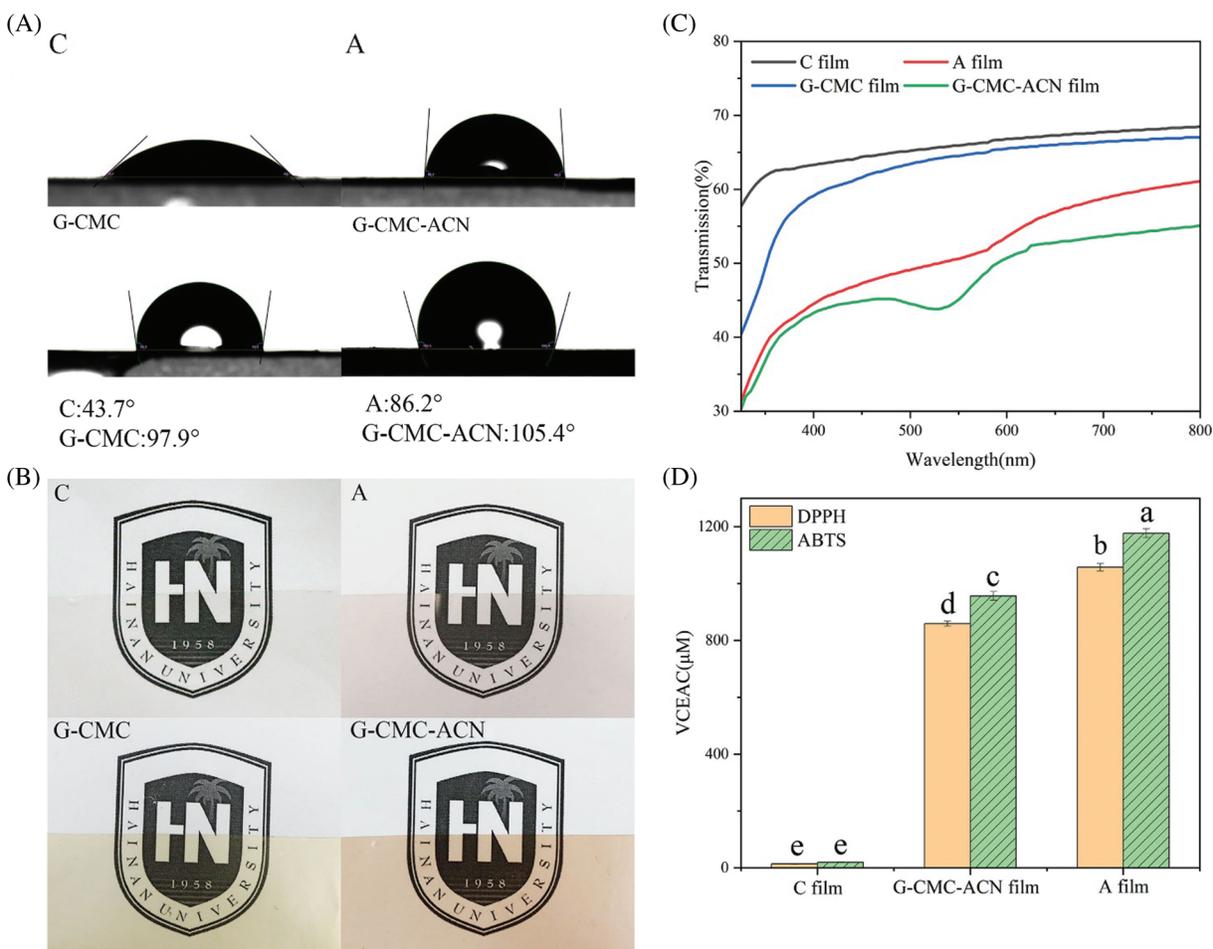
**Figure 3:** Water contact angle of films (A). Color of films (B). Ultraviolet–visible (UV–vis) light transmittance (C) of films. Antioxidant activity of films (D)

### 3.3.6 Color and Light Transmission

Color is crucial for the application of pH-responsive smart film [39]. The colors and parameters (L*, a*, b*, and ΔE) for each of the four films are shown in Fig. 3B and Table 3. L represents the brightness, +a* and −a* indicate red and green, +b* and −b* represent yellow and blue, respectively, and ΔE represents the color difference from the white standard color plate. The corn starch film, without additives, was visually transparent. After adding free ACN, the film turned dark purple and the brightness decreased (L = 87.88 → L = 81.81). The G-CMC film's pale yellowish hue was brought on by glutenin, and the orange color of the G-CMC-ACN film was due to the combined effect of the encapsulated ACNs and glutenin.

Films used to package food must be capable of blocking UV–vis light, because UV–vis light causes food oxidation and a reduction in shelf life [47]. By measuring light transmittance, the films' ability to block light was assessed. The light transmittances of the four films from highest to lowest were: C, G-CMC, A, and G-CMC-ACN (Fig. 3C). The light transmission of the G-CMC film was lower than that of the C film, which indicates that the homogeneous G-CMC nanocomplex distribution leads to light scattering and reflection [23]. The light transmittances of the A and G-CMC-ACN films were significantly lower than that of the C and G-CMC films. This may be caused by ACNs' aromatic rings absorbing the UV–vis light. Owing

to the light being absorbed by flavonoid cations in the 500–600 nm range, the A and G-CMC-ACN films' transmittances significantly decreased.

**Table 3:** Color parameters of films

| Films | L* | a* | b* | $\Delta E$ |
|---|---|---|---|---|
| C film | 87.88 ± 0.08a | 1.89 ± 0.05c | −7.67 ± 0.06d | 13.62 ± 0.06d |
| A film | 81.81 ± 0.13c | 4.86 ± 0.08b | −4.51 ± 0.07c | 18.09 ± 0.15b |
| G-CMC film | 83.03 ± 0.23b | 1.29 ± 0.03d | 6.01 ± 0.38a | 16.02 ± 0.12c |
| G-CMC-ACN film | 77.99 ± 0.24d | 10.58 ± 0.13a | 2.53 ± 0.14b | 23.20 ± 0.28a |

Note: Different letters in the same column indicate significant differences ($p < 0.05$).

### 3.3.7 Antioxidant Properties

The antioxidant properties of films were determined by calculating the vitamin C equivalent antioxidant capacity (Fig. 3D). Compared with pure starch films, free ACN-containing films and ACN-loaded nanocomplex films showed significantly higher antioxidant activity. ACNs are polyphenols, which contain numerous phenolic hydroxyl groups that form phenoxy groups by eliminating free radicals, improving the antioxidant activity compared with that of pure starch films [48]. The free ACN-containing films had higher antioxidant properties than the nanocomplex films, because the antioxidant property of ACNs was reduced by nanocomplex encapsulation. This caused the release of encapsulated ACNs to be slower. The antioxidant property of the composite films depended not only on the ACN release from the film, but also on the microstructure and release environment of the film. Qin et al. also found that films containing free ACNs had higher antioxidant activity [12]. Therefore, ACN-loaded nanocomplex films could be used not only in smart packaging to monitor freshness, but also in active packaging to extend the shelf life of food [49].

### 3.3.8 Thermal Properties

The thermal properties of the films were investigated using thermogravimetric analysis. All films exhibited three decomposition stages (Fig. 4): (1) 50°C–170°C, where the mass loss was caused by water evaporation; (2) 250°C–330°C, thought to be due to the degradation of polysaccharides, proteins, starches, and plasticizers in the film; and (3) >350°C, when decomposition occurred primarily because of glycosidic bond degradation and further decomposition of intermediate products [50]. The residual weight of the starch films containing the nanocomplexes was significantly higher than those without nanocomplexes, which indicated that nanocomplexes could noticeably enhance the thermal stability of starch films [51]. Pure starch films have only one degradation mechanism; however, a second type of degradation was observed in both nanocomplex films. It is presumed that the nanocomplexes are partially degraded at relatively low temperatures and the primary structures begin to dissociate at 305°C. In typical usage of the packaging, the ambient temperature remained below 100°C, thereby indicating that the stable film may fulfill the requirements for food packaging.

### 3.3.9 Color Reaction in Different pH Environments

Table 4 presents the colors and parameters of the G-CMC-ACNs films in the pH range of 2–12. The film was pH sensitive and demonstrated a significant color change. The findings demonstrate that the G-CMC-ACN film's color change trend was comparable to that of the ACN solution. The color of the film transformed from red (pH 2.0) to pink (pH 3.0–4.0), light yellow (pH 5.0–7.0), greyish purple (pH 8.0–10.0), and finally light green (pH 11.0–12.0) as the pH increased. The a* value decreased, whereas the b* value increased, then decreased, and then increased again, indicating a change in film color from red to chartreuse with an increase in the pH. Owing to the ACNs' structural changes at various pH levels, the film's color changed in different pH buffers [52].

(A)



(B)
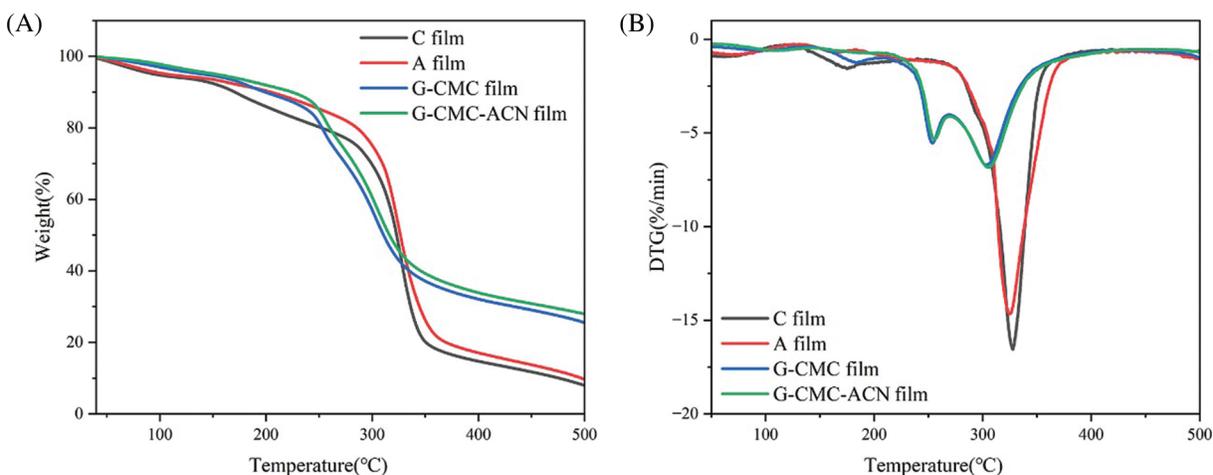
**Figure 4:** TGA (A) and DTG (B) curves for all films

**Table 4:** Color parameters and photographs of G-CMC-ACNs film in pH 2.0–12.0 buffers

| pH | Film photo | L* | a* | b* | ΔE |
|----|-----------|-----|-----|-----|-----|
| 2  | | 63.08 ± 0.50h | 13.76 ± 0.21a | 2.58 ± 0.09e | 37.98 ± 0.47a |
| 3  | | 64.81 ± 0.37g | 10.87 ± 0.28b | 3.54 ± 0.10cd | 35.38 ± 0.38c |
| 4  | | 64.97 ± 0.46g | 8.87 ± 0.18c | 4.60 ± 0.09b | 34.71 ± 0.46cd |
| 5  | | 69.60 ± 0.33e | 6.42 ± 0.24d | 5.61 ±0.26a | 29.76 ± 0.26f |
| 6  | | 73.59 ± 0.15c | 4.76 ± 0.28e | 4.69 ± 0.33b | 25.40 ± 0.08fg |
| 7  | | 75.73 ± 0.39b | 3.50 ± 0.32f | 3.31 ± 0.18d | 22.88 ± 0.33h |
| 8  | | 77.07 ± 0.24a | 2.51 ± 0.07g | 1.31 ± 0.09f | 21.26 ± 0.25i |
| 9  | | 72.79 ± 0.11d | 1.96 ± 0.20g | 0.75 ± 0.17g | 25.43 ± 0.12g |
| 10 | | 67.07 ± 0.31f | −0.41 ± 0.28h | 1.47 ± 0.19f | 30.98 ± 0.31e |
| 11 | | 61.39 ± 0.24i | −1.61 ± 0.25i | 2.29 ± 0.15e | 36.69 ± 0.24b |
| 12 | | 63.66 ± 0.07h | −3.64 ± 0.14j | 3.87 ± 0.13c | 34.61 ± 0.07d |
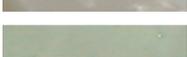
Note: Different letters in the same column indicate significant differences ($p < 0.05$).

### 3.4 Application of the Films

Based on the color response of G-CMC-ACN films to different pH solutions, the film was applied to real-time monitoring of the freshness of chilled pork. The freshness of the pork during storage was evaluated comprehensively by measuring the weight loss, pH, and TVB-N content. With increased storage time, the weight loss rate increased, pH first decreased and then increased, and the TVB-N

content increased (Table 5). The pH decreased during the stiff period when adenosine triphosphate and glycogen break down to form lactate and phosphate, respectively. Subsequently, bacteria and enzymes break down the proteins to produce alkaline nitrogenous substances, such as TVB-N, resulting in an increase in the pH. Based on TVB-N content, pork can be divided into three grades: Fresh (<15 mg/100 g), secondary fresh (15–25 mg/100 g), and corrupted (>25 mg/100 g). Pork can also be classified into the following three classes based on pH changes: fresh (5.8–6.2), secondary fresh (6.3–6.6) and corrupted (>6.7). We observed that pork was still fresh between 0 and 2 days, secondary fresh between 4 and 6 days, and began to rot after 8 days of storage. The color of the ACN-loaded nanocomplex films changed depending on how fresh the pork was (Fig. 5). The color transformed from orange (0–2 days) to pink (4–6 days) and finally, to chartreuse (8–10 days). This is the visible color change, reflected by the color parameters a* (9.35 → 12.19 → −1.6) and b* (2.43 → 1.06 → 2.74). Orange, pink, and chartreuse represented the fresh, secondary fresh, and putrefaction states of pork, respectively, indicating that there was good agreement between the films and the stages noted. Zhang et al. also showed that ACN-loaded films could indicate pork spoilage based on the color of the film [53]. Therefore, the ACN-loaded nanocomplex film can be used to monitor the freshness of pork [54].

**Table 5:** Changes in pH, weight loss, TVB-N content, and color parameters of chilled pork at different storage times

| Storage time (d) | pH | Weight loss (%) | TVB-N contents (mg/100 g) | L* | a* | b* |
|---|---|---|---|---|---|---|
| 0 | 5.63 ± 0.02e | 0.00f | 7.96 ± 0.33f | 78.68 ± 0.52a | 9.35 ± 0.17c | 2.43 ± 0.08ab |
| 2 | 5.52 ± 0.02f | 4.46 ± 0.55e | 9.04 ± 0.55e | 62.45 ± 0.49b | 9.28 ± 0.32c | 2.19 ± 0.08bc |
| 4 | 5.79 ± 0.03d | 5.89 ± 0.68d | 14.33 ± 0.14d | 64.71 ± 0.26c | 10.14 ± 0.12b | 1.51 ± 0.21d |
| 6 | 6.03 ± 0.05c | 7.89 ± 0.49c | 19.77 ± 0.55c | 64.69 ± 0.34c | 12.19 ± 0.13a | 1.06 ± 0.11e |
| 8 | 6.44 ± 0.03b | 9.92 ± 0.66b | 23.60 ± 0.43b | 62.83 ± 0.41b | 5.05 ± 0.29d | 2.03 ± 0.15c |
| 10 | 6.70 ± 0.02a | 11.92 ± 0.74a | 26.95 ± 0.90a | 58.72 ± 0.45d | −1.60 ± 0.26e | 2.74 ± 0.10a |

Note: Different letters in the same column indicate significant differences ($p < 0.05$).
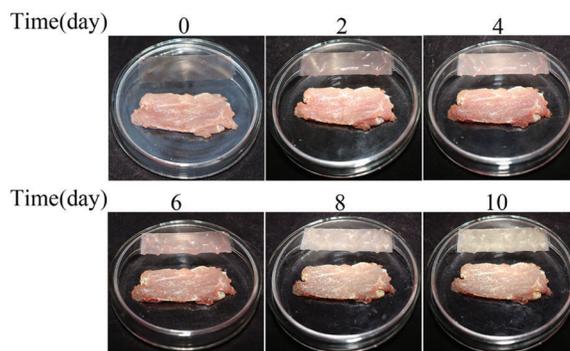


**Figure 5:** Transformation of pork and films during storage

## 4  Conclusion

Smart colorimetric films of G-CMC-ACN nanocomplexes held in corn starch matrices were developed and used to monitor the freshness of chilled pork in real time. G-CMC-ACN films showed improved mechanical properties, light-shielding ability, hydrophobicity, lower water vapor transmission, and excellent resistance to oxidation and pH, as compared with traditional smart films. This can be attributed to their good biocompatibility and the creation of new hydrogen bonds between the G-CMC-ACN nanocomplexes and corn starch film matrix. In practical applications, G-CMC-ACNs films can monitor the freshness of chilled pork in real time through color changes that are visible to the naked eye. Thus, the biodegradable G-CMC-ACN film has promising potential in food packaging applications.

**Author Contributions:** Study conception and design: Juan Yan, Wenchao Li; data collection: Juan Yan, Xianfang Zhang; analysis and interpretation of results: Juan Yan, Wenchao Li. Shisheng Liu; draft manuscript preparation: Juan Yan, Shisheng Liu. All authors reviewed the results and approved the final version of the manuscript.

**Conflicts of Interest:** The authors declare that they have no conflicts of interest to report regarding the present study.

## References

1. Flórez, M., Guerra-Rodríguez, E., Cazón, P., Vázquez, M. (2022). Chitosan for food packaging: Recent advances in active and intelligent films. *Food Hydrocolloids, 124(4),* 107328. https://doi.org/10.1016/j.foodhyd.2021.107328

2. Ochoa-Yepes, O., Di Giogio, L., Goyanes, S., Mauri, A., Famá, L. (2019). Influence of process (extrusion/thermo-compression, casting) and lentil protein content on physicochemical properties of starch films. *Carbohydrate Polymers, 208(5–6),* 221–231. https://doi.org/10.1016/j.carbpol.2018.12.030

3. Cortés-Rodríguez, M., Villegas-Yépez, C., Gil González, J. H., Rodríguez, P. E., Ortega-Toro, R. (2020). Development and evaluation of edible films based on cassava starch, whey protein, and bees wax. *Heliyon, 6(9),* e04884. https://doi.org/10.1016/j.heliyon.2020.e04884

4. Sultan, M., Abdelhakim, A. A., Nassar, M., Hassan, Y. R. (2023). Active packaging of chitosan film modified with basil oil encapsulated in silica nanoparticles as an alternate for plastic packaging materials. *Food Bioscience, 51,* 102298. https://doi.org/10.1016/j.fbio.2022.102298

5. Karimi Sani, I., Masoudpour-Behabadi, M., Alizadeh Sani, M., Motalebinejad, H., Juma, A. S. M. et al. (2023). Value-added utilization of fruit and vegetable processing by-products for the manufacture of biodegradable food packaging films. *Food Chemistry, 405(6),* 134964. https://doi.org/10.1016/j.foodchem.2022.134964

6. Alizadeh-Sani, M., Mohammadian, E., Rhim, J. W., Jafari, S. M. (2020). pH-sensitive (halochromic) smart packaging films based on natural food colorants for the monitoring of food quality and safety. *Trends in Food Science & Technology, 105(19),* 93–144. https://doi.org/10.1016/j.tifs.2020.08.014

7. Amin, U., Khan, M. K. I., Maan, A. A., Nazir, A., Riaz, S. et al. (2022). Biodegradable active, intelligent, and smart packaging materials for food applications. *Food Packaging and Shelf Life, 33(4),* 100903. https://doi.org/10.1016/j.fpsl.2022.100903

8. Yong, H., Liu, J. (2020). Recent advances in the preparation, physical and functional properties, and applications of anthocyanins-based active and intelligent packaging films. *Food Packaging and Shelf Life, 26,* 100550. https://doi.org/10.1016/j.fpsl.2020.100550

9. Neves, D., Andrade, P. B., Videira, R. A., de Freitas, V., Cruz, L. (2022). Berry anthocyanin-based films in smart food packaging: A mini-review. *Food Hydrocolloids, 133,* 107885. https://doi.org/10.1016/j.foodhyd.2022.107885

10. Yang, W., Guo, Y., Liu, M., Chen, X., Xiao, X. et al. (2022). Structure and function of blueberry anthocyanins: A review of recent advances. *Journal of Functional Foods, 88(2),* 104864. https://doi.org/10.1016/j.jff.2021.104864

11. Zhao, L., Liu, Y., Zhao, L., Wang, Y. (2022). Anthocyanin-based pH-sensitive smart packaging films for monitoring food freshness. *Journal of Agriculture and Food Research, 9,* 100340. https://doi.org/10.1016/j.jafr.2022.100340

12. Qin, Y., Yun, D., Xu, F., Chen, D., Kan, J. et al. (2021). Smart packaging films based on starch/polyvinyl alcohol and Lycium ruthenicum anthocyanins-loaded nano-complexes: Functionality, stability and application. *Food Hydrocolloids, 119,* 106850. https://doi.org/10.1016/j.foodhyd.2021.106850

13. Bao, C., Jiang, P., Chai, J., Jiang, Y., Li, D. et al. (2019). The delivery of sensitive food bioactive ingredients: Absorption mechanisms, influencing factors, encapsulation techniques and evaluation models. *Food Research International, 120(15),* 130–140. https://doi.org/10.1016/j.foodres.2019.02.024

14. Cui, H., Si, X., Tian, J., Lang, Y., Gao, N. et al. (2022). Anthocyanins-loaded nanocomplexes comprising casein and carboxymethyl cellulose: Stability, antioxidant capacity, and bioaccessibility. *Food Hydrocolloids, 122(2),* 107073. https://doi.org/10.1016/j.foodhyd.2021.107073

15. Zhang, X., Zeng, Q., Liu, Y., Cai, Z. (2021). Enhancing the resistance of anthocyanins to environmental stress by constructing ovalbumin-propylene glycol alginate nanocarriers with novel configurations. *Food Hydrocolloids, 118(2),* 106668. https://doi.org/10.1016/j.foodhyd.2021.106668

16. Jamróz, E., Tkaczewska, J., Kopeć, M., Cholewa-Wójcik, A. (2022). Shelf-life extension of salmon using active total biodegradable packaging with tea ground waste and furcellaran-CMC double-layered films. *Food Chemistry, 383(3),* 132425. https://doi.org/10.1016/j.foodchem.2022.132425

17. Widyarani, Ratnaningsih, E., Sanders, J. P. M., Bruins, M. E. (2014). Biorefinery methods for separation of protein and oil fractions from rubber seed kernel. *Industrial Crops and Products, 62,* 323–332. https://doi.org/10.1016/j.indcrop.2014.09.005

18. Zhou, W., He, Y., Liu, F., Liao, L., Huang, X. et al. (2021). Carboxymethyl chitosan-pullulan edible films enriched with galangal essential oil: Characterization and application in mango preservation. *Carbohydrate Polymers, 256(3),* 117579. https://doi.org/10.1016/j.carbpol.2020.117579

19. Karimi, T., Mottaghitalab, F., Keshvari, H., Farokhi, M. (2023). Carboxymethyl chitosan/sodium carboxymethyl cellulose/agarose hydrogel dressings containing silk fibroin/polydopamine nanoparticles for antibiotic delivery. *Journal of Drug Delivery Science and Technology, 80,* 104134. https://doi.org/10.1016/j.jddst.2022.104134

20. Ge, J., Yue, P., Chi, J., Liang, J., Gao, X. (2018). Formation and stability of anthocyanins-loaded nanocomplexes prepared with chitosan hydrochloride and carboxymethyl chitosan. *Food Hydrocolloids, 74(1),* 23–31. https://doi.org/10.1016/j.foodhyd.2017.07.029

21. Mary, S. K., Koshy, R. R., Arunima, R., Thomas, S., Pothen, L. A. (2022). A review of recent advances in starch-based materials: Bionanocomposites, pH sensitive films, aerogels and carbon dots. *Carbohydrate Polymer Technologies and Applications, 3,* 100190. https://doi.org/10.1016/j.carpta.2022.100190

22. Agarwal, S. (2021). Major factors affecting the characteristics of starch based biopolymer films. *European Polymer Journal, 160(2),* 110788. https://doi.org/10.1016/j.eurpolymj.2021.110788

23. Liu, L., Wu, W., Zheng, L., Yu, J., Sun, P. et al. (2022). Intelligent packaging films incorporated with anthocyanins-loaded ovalbumin-carboxymethyl cellulose nanocomplexes for food freshness monitoring. *Food Chemistry, 387(2),* 132908. https://doi.org/10.1016/j.foodchem.2022.132908

24. He, B., Ge, J., Yue, P., Yue, X., Fu, R. et al. (2017). Loading of anthocyanins on chitosan nanoparticles influences anthocyanin degradation in gastrointestinal fluids and stability in a beverage. *Food Chemistry, 221(1),* 1671–1677. https://doi.org/10.1016/j.foodchem.2016.10.120

25. Feng, L., Liu, H., Li, L., Wang, X., Kitazawa, H. et al. (2022). Improving the property of a reproducible bioplastic film of glutenin and its application in retarding senescence of postharvest *Agaricus bisporus. Food Bioscience, 48(2),* 101796. https://doi.org/10.1016/j.fbio.2022.101796

26. Sartori, T., Feltre, G., do Amaral Sobral, P. J., Lopes da Cunha, R., Menegalli, F. C. (2018). Properties of films produced from blends of pectin and gluten. *Food Packaging and Shelf Life, 18(2),* 221–229. https://doi.org/10.1016/j.fpsl.2018.11.007

27. Xiao, M., Tang, B., Qin, J., Wu, K., Jiang, F. (2022). Properties of film-forming emulsions and films based on corn starch/sodium alginate/gum Arabic as affected by virgin coconut oil content. *Food Packaging and Shelf Life, 32(4),* 100819. https://doi.org/10.1016/j.fpsl.2022.100819

28. Dong, M., Tian, L., Li, J., Jia, J., Dong, Y. et al. (2022). Improving physicochemical properties of edible wheat gluten protein films with proteins, polysaccharides and organic acid. *LWT, 154(5),* 112868. https://doi.org/10.1016/j.lwt.2021.112868

29. Li, W., Gong, P., Ma, H., Xie, R., Wei, J. et al. (2022). Ultrasound treatment degrades, changes the color, and improves the antioxidant activity of the anthocyanins in red radish. *LWT, 165(4),* 113761. https://doi.org/10.1016/j.lwt.2022.113761

30. Shi, C., Ji, Z., Zhang, J., Jia, Z., Yang, X. (2022). Preparation and characterization of intelligent packaging film for visual inspection of tilapia fillets freshness using cyanidin and bacterial cellulose. *International Journal of Biological Macromolecules, 205,* 357–365. https://doi.org/10.1016/j.ijbiomac.2022.02.072

31. Yun, D., Cai, H., Liu, Y., Xiao, L., Song, J. et al. (2019). Development of active and intelligent films based on cassava starch and Chinese bayberry (*Myrica rubra* Sieb. et Zucc.) anthocyanins. *RSC Advances, 9(53),* 30905–30916. https://doi.org/10.1039/C9RA06628D

32. Etxabide, A., Kilmartin, P. A., Maté, J. I. (2021). Color stability and pH-indicator ability of curcumin, anthocyanin and betanin containing colorants under different storage conditions for intelligent packaging development. *Food Control, 121,* 107645. https://doi.org/10.1016/j.foodcont.2020.107645

33. Cheng, M., Cui, Y., Yan, X., Zhang, R., Wang, J. et al. (2022). Effect of dual-modified cassava starches on intelligent packaging films containing red cabbage extracts. *Food Hydrocolloids, 124(1),* 107225. https://doi.org/10.1016/j.foodhyd.2021.107225

34. Sun, C., Dai, L., Gao, Y. (2017). Formation and characterization of the binary complex between zein and propylene glycol alginate at neutral pH. *Food Hydrocolloids, 64(45),* 36–47. https://doi.org/10.1016/j.foodhyd.2016.10.031

35. Tomé Constantino, A. B., Garcia-Rojas, E. E. (2022). Microencapsulation of betanin by complex coacervation of carboxymethylcellulose and amaranth protein isolate for application in edible gelatin films. *Food Hydrocolloids, 133(9),* 107956. https://doi.org/10.1016/j.foodhyd.2022.107956

36. Zhai, X., Shi, J., Zou, X., Wang, S., Jiang, C. et al. (2017). Novel colorimetric films based on starch/polyvinyl alcohol incorporated with roselle anthocyanins for fish freshness monitoring. *Food Hydrocolloids, 69(3),* 308–317. https://doi.org/10.1016/j.foodhyd.2017.02.014

37. Ma, Y., Zhao, Y., Xie, J., Sameen, D. E., Ahmed, S. et al. (2021). Optimization, characterization and evaluation of papaya polysaccharide-corn starch film for fresh cut apples. *International Journal of Biological Macromolecules, 166,* 1057–1071. https://doi.org/10.1016/j.ijbiomac.2020.10.261

38. Medina-Jaramillo, C., Bernal, C., Famá, L. (2019). Influence of green tea and basil extracts on cassava starch based films as assessed by thermal degradation, crystalline structure and mechanical properties. *Starch—Starke, 72(3–4),* 1900155. https://doi.org/10.1002/star.201900155

39. Susmitha, A., Sasikumar, K., Rajan, D., Padmakumar, M., Nampoothiri, A. et al. (2021). Development and characterization of corn starch-gelatin based edible films incorporated with mango and pineapple for active packaging. *Food Bioscience, 41(1),* 100977. https://doi.org/10.1016/j.fbio.2021.100977

40. Huang, J., Chen, M., Zhou, Y., Li, Y., Hu, Y. (2020). Functional characteristics improvement by structural modification of hydroxypropyl methylcellulose modified polyvinyl alcohol films incorporating roselle anthocyanins for shrimp freshness monitoring. *International Journal of Biological Macromolecules, 162,* 1250–1261. https://doi.org/10.1016/j.ijbiomac.2020.06.156

41. Guo, Z., Huang, Y., Huang, J., Li, S., Zhu, Z. et al. (2022). Formation of protein-anthocyanin complex induced by grape skin extracts interacting with wheat gliadins: Multi-spectroscopy and molecular docking analysis. *Food Chemistry, 385(2),* 132702. https://doi.org/10.1016/j.foodchem.2022.132702

42. Jiang, G., Hou, X., Zeng, X., Zhang, C., Wu, H. et al. (2020). Preparation and characterization of indicator films from carboxymethyl-cellulose/starch and purple sweet potato (*Ipomoea batatas* (L.) lam) anthocyanins for monitoring fish freshness. *International Journal of Biological Macromolecules, 143(1),* 359–372. https://doi.org/10.1016/j.ijbiomac.2019.12.024

43. Thuy, N., Le, H. H., Vy, T. T., Tam, N., Thanh, T. L. et al. (2021). Green synthesis of silver nanoparticles using plectranthus amboinicus leaf extract for preparation of CMC/PVA nanocomposite film. *Journal of Renewable Materials, 9(8),* 1393–1411. https://doi.org/10.32604/jrm.2021.015772

44. Yao, X., Liu, J., Hu, H., Yun, D., Liu, J. (2022). Development and comparison of different polysaccharide/PVA-based active/intelligent packaging films containing red pitaya betacyanins. *Food Hydrocolloids, 124,* 107305. https://doi.org/10.1016/j.foodhyd.2021.107305

45. Yan, J., Li, M., Wang, H., Lian, X., Fan, Y. et al. (2021). Preparation and property studies of chitosan-PVA biodegradable antibacterial multilayer films doped with $Cu_2O$ and nano-chitosan composites. *Food Control, 126(6),* 108049. https://doi.org/10.1016/j.foodcont.2021.108049

46. Boccalon, E., Viscusi, G., Lamberti, E., Fancello, F., Zara, S. et al. (2022). Composite films containing red onion skin extract as intelligent pH indicators for food packaging. *Applied Surface Science, 593(2),* 153319. https://doi.org/10.1016/j.apsusc.2022.153319

47. Cao, T. L., Song, K. B. (2019). Effects of gum karaya addition on the characteristics of loquat seed starch films containing oregano essential oil. *Food Hydrocolloids, 97(11),* 105198. https://doi.org/10.1016/j.foodhyd.2019.105198

48. Qin, Y., Liu, Y., Yong, H., Liu, J., Liu, J. (2019). Preparation and characterization of active and intelligent packaging films based on cassava starch and anthocyanins from *Lycium ruthenicum* Murr. *International Journal of Biological Macromolecules, 134,* 80–90. https://doi.org/10.1016/j.ijbiomac.2019.05.029

49. Wang, S., Xia, P., Wang, S., Liang, J., Sun, Y. et al. (2019). Packaging films formulated with gelatin and anthocyanins nanocomplexes: Physical properties, antioxidant activity and its application for olive oil protection. *Food Hydrocolloids, 96(15),* 617–624. https://doi.org/10.1016/j.foodhyd.2019.06.004

50. Ren, Y., Wu, Z., Shen, M., Rong, L., Liu, W. et al. (2021). Improve properties of sweet potato starch film using dual effects: Combination mesona Chinensis benth polysaccharide and sodium carbonate. *LWT, 140(2),* 110679. https://doi.org/10.1016/j.lwt.2020.110679

51. Zhao, S., Jia, R., Yang, J., Dai, L., Ji, N. et al. (2022). Development of chitosan/tannic acid/corn starch multifunctional bilayer smart films as pH-responsive actuators and for fruit preservation. *International Journal of Biological Macromolecules, 205,* 419–429. https://doi.org/10.1016/j.ijbiomac.2022.02.101

52. da Silva Filipini, G., Romani, V. P., Guimarães Martins, V. (2020). Biodegradable and active-intelligent films based on methylcellulose and jambolão (*Syzygium cumini*) skins extract for food packaging. *Food Hydrocolloids, 109,* 106139. https://doi.org/10.1016/j.foodhyd.2020.106139

53. Zhang, X., Zou, W., Xia, M., Zeng, Q., Cai, Z. (2021). Intelligent colorimetric film incorporated with anthocyanins-loaded ovalbumin-propylene glycol alginate nanocomplexes as a stable pH indicator of monitoring pork freshness. *Food Chemistry, 368(2),* 130825. https://doi.org/10.1016/j.foodchem.2021.130825

54. Tahir, H. E., Hashim, S. B. H., Komla Mahunu, G., Arslan, M., Jiyong, S. et al. (2022). Smart films fabricated from natural pigments for measurement of total volatile basic nitrogen (TVB-N) content of meat for freshness evaluation: A systematic review. *Food Chemistry, 396(5),* 133674. https://doi.org/10.1016/j.foodchem.2022.133674